International Journal of Thermophysics, Vol. 23, No. 5, September 2002 (© 2002)

A Fast Laser Polarimeter Improving a Microsecond Pulse Heating System[1]

A. Seifter,[2] F. Sachsenhofer,[2] and G. Pottlacher[2, 3]

The microsecond pulse heating system has been used for more than 15 years to investigate thermophysical properties of solid and liquid metals and alloys. The only way to measure temperature in the time and temperature range of these experiments (duration of a few tens of microseconds, temperatures up to 7000 K) is optical pyrometry. The radiance temperature can be measured very accurately. However, to obtain true temperature from radiance temperature the normal spectral emissivity at the wavelength of interest of the material under investigation has to be known. Because normal spectral emissivity measurements on pulse heated liquid metals were not possible in the past, an assumption about the behavior of the emissivity in the liquid phase had to be made, which increased the uncertainty of the temperature determination. To overcome this limitation in temperature measurement, a microsecond division of amplitude polarimeter (μ-DOAP) was added to the pulse heating system. The normal spectral emissivity at 684.5 nm is derived from the measured change in the state of polarization of laser light that is reflected off the sample surface. The working principle of this polarimeter system is presented, and experimental results of the normal spectral emissivity at 684.5 nm as a function of radiance temperature at 650 nm are discussed.

KEY WORDS: emissivity; liquid metals, polarimetry; pulse heating; pyrometry.

1. INTRODUCTION

Using a calibrated pyrometer the radiance temperature of hot surfaces can be determined very accurately. However, to obtain true temperature from

[1] Paper presented at the Sixth International Workshop on Subsecond Thermophysics, September 26–28, 2001, Leoben, Austria.

[2] Institut für Experimentalphysik, Technische Universität Graz, Petersgasse 16, A-8010 Graz, Austria.

[3] To whom correspondence should be addressed. E-mail: pottl@iep.tu-graz.ac.at

0195-928X/02/0900-1267/0 © 2002 Plenum Publishing Corporation

this quantity, the sample's normal spectral emissivity at the operating wavelength of the pyrometer has to be known, otherwise large errors can occur [1]. In the past the assumption of a constant emissivity of the liquid sample over the entire temperature range of interest was usually made. To eliminate this source of uncertainty a polarimetric method for the direct measurement of normal spectral emissivity at high temperatures (above 1500 K) and very short timescales (duration of an experiment about 30 μs) has been integrated into the existing experimental setup.

The division of amplitude photopolarimeter (μ-DOAP) detects changes in the polarization state of a laser beam ($\lambda = 684.5$ nm) that is reflected off the sample surface during the pulse—heating experiments. The change in the polarization state is used to determine the index of refraction n and the extinction coefficient k of the sample. This leads to the reflectivity $\Re$ of the sample and, by means of Kirchhoff's law for opaque materials, to its normal spectral emissivity.

Due to the short duration of the experiments, the polarimeter has to operate without any moving parts. This is done by dividing the reflected laser beam, using suitable optical components, into four beams and measuring their intensities. With the aid of the instrument matrix (a 4×4-array, obtained via calibration), the Stokes vector and, hence, complete information about the polarization state of the reflected beam, is obtained.

2. POLARIZED LIGHT/STOKES FORMALISM

All polarization states can be generated by the superposition of two orthogonal polarization states (horizontal and vertical linearly polarized, +45° and −45° linearly polarized, right- and left-handed circularly polarized) with the intensities I_1 and I_2 and a phase difference δ. Looking toward the source of the polarized wave, the terminus of the electric field vector, in general, traces an ellipse (Fig. 1), called the polarization ellipse, which can be described by its ellipticity angle ε_a and azimuth ψ [2].

Since these parameters are not accessible to a direct measurement, it is simpler to describe the polarization state of an electromagnetic wave by means of the four-component Stokes vector $\vec{S}$:

$$\vec{S} = \begin{pmatrix} S_0 \\ S_1 \\ S_2 \\ S_3 \end{pmatrix} = \begin{pmatrix} I_{\text{tot}} \\ I_{\text{h}} - I_{\text{v}} \\ I_{+45} - I_{-45} \\ I_{\text{rcp}} - I_{\text{lcp}} \end{pmatrix} = I_{\text{tot}} \begin{pmatrix} 1 \\ \cos 2\psi \cdot \cos 2\varepsilon_a \\ \sin 2\psi \cdot \cos 2\varepsilon_a \\ \sin 2\varepsilon_a \end{pmatrix} \tag{1}$$

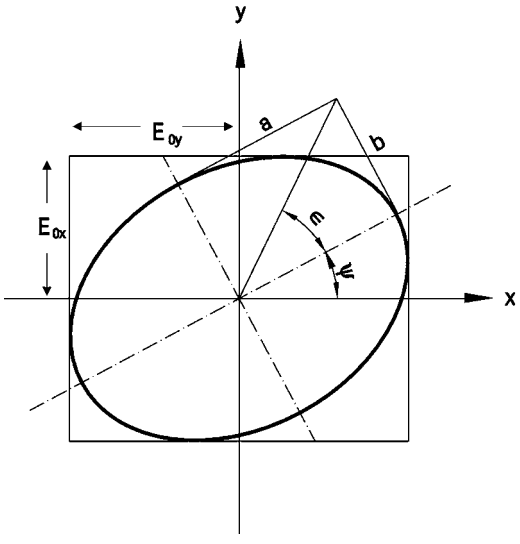

Fig. 1. Polarization ellipse. $E_{0x,\,0y}$, amplitudes of the electric field; a, b, axes of the ellipse; ε_a, ellipticity angle; ψ, azimuth.

with S_{0-3}, Stokes parameters; I_{tot}, total intensity; $I_{h,\,v}$, intensity of the horizontal and vertical linearly polarized components; $I_{+45,\,-45}$, intensity of the $+45°$ and $-45°$ linearly polarized components; and $I_{rcp,\,lcp}$, intensity of the right-handed and left-handed circularly polarized components.

Using this vector any polarization state can be described by the intensity of two orthogonal components, whose superposition produces the corresponding state. This formalism can be used to describe partially polarized light with a degree of polarization deg P, defined as

$$\deg P = \frac{[S_1^2 + S_2^2 + S_3^2]^{1/2}}{S_0} \leqslant 1 \tag{2}$$

3. INTERACTION OF LIGHT WITH MATTER

The change in the polarization state of light that is reflected at the planar interface between two optically isotropic, semi-infinite homogeneous media is described by Fresnel's equations:

$$r_{\mathrm{p}} = \frac{R_{\mathrm{p}}}{A_{\mathrm{p}}} = \frac{n_2 \cos \Theta_{\mathrm{i}} - n_1 \cos \Theta_{\mathrm{t}}}{n_2 \cos \Theta_{\mathrm{i}} + n_1 \cos \Theta_{\mathrm{t}}} \tag{3}$$

$$r_{\mathrm{n}} = \frac{R_{\mathrm{n}}}{A_{\mathrm{n}}} = \frac{n_1 \cos \Theta_{\mathrm{i}} - n_2 \cos \Theta_{\mathrm{t}}}{n_1 \cos \Theta_{\mathrm{i}} + n_2 \cos \Theta_{\mathrm{t}}} \tag{4}$$

with $r_{\mathrm{p,n}}$, = Fresnel coefficients for the electric field parallel and normal to the plane of incidence; $n_{1,2}$, = refractive indices of the two media; $\Theta_{\mathrm{i,t}}$, angles of incidence and refraction; and $R_{\mathrm{n,p}}$ and $A_{\mathrm{n,p}}$, = the complex amplitudes of the electric field normal and parallel to the plane of incidence (see Fig. 2).

These equations are derived from Maxwell's equations and the boundary conditions for electromagnetic waves [3]. In the case of an electrical conductor with an electrical conductivity σ as the reflecting medium, the real dielectric constant ε_{e} is replaced by the complex dielectric constant $\hat{\varepsilon}_{\mathrm{e}}$

$$\hat{\varepsilon}_{\mathrm{e}} = \varepsilon_{\mathrm{e}} - i \frac{\sigma}{\varepsilon_0 \omega} \tag{5}$$

where ω is the angular frequency and ε_0 is the static dielectric constant.

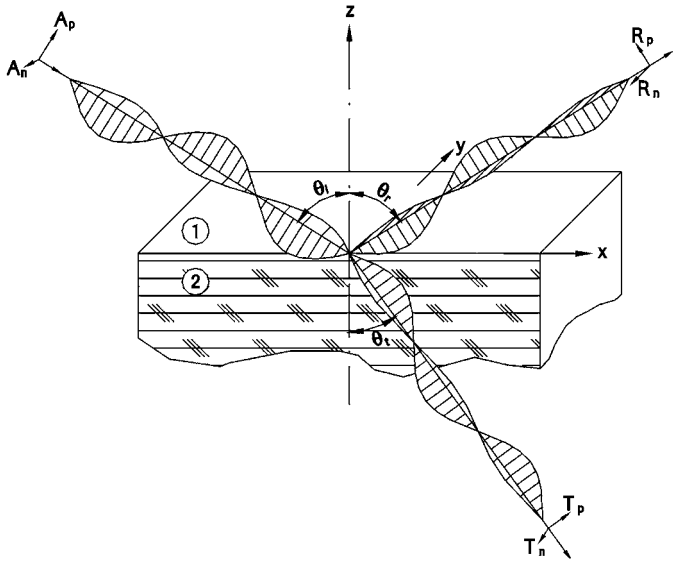

Fig. 2. Interaction of light with matter. $A_{\mathrm{n,p}}$, amplitudes of the incident light normal and parallel to the plane of incidence; $R_{\mathrm{n,p}}$, amplitudes of the reflected light normal and parallel to the plane of incidence; $T_{\mathrm{n,p}}$, amplitudes of the refracted light normal and parallel to the plane of incidence; $\Theta_{\mathrm{i,r,t}}$, angle of incidence, reflection and refraction.

The complex index of refraction $\hat{n}$ of this medium is obtained using

$$\hat{n} = \sqrt{\mu \hat{\varepsilon}_e} = n - ik \tag{6}$$

where μ is the magnetic permeability (~ 1 for metals); n is the real part of the complex index of refraction; and k is the extinction coefficient.

Thus, in this case the Fresnel coefficients r_p and r_n are complex and, in addition, a phase shift is introduced between the components of the reflected wave that are linearly polarized normal (subscript n) and parallel (subscript p) to the plane of incidence. The complex Fresnel coefficients can be expressed in terms of an amplitude ρ and a phase φ:

$$\hat{r}_p = \frac{R_p}{A_p} = \rho_p e^{i\phi_p} \tag{7a}$$

$$\hat{r}_n = \frac{R_n}{A_n} = \rho_n e^{i\phi_n} \tag{7b}$$

The ellipsometric parameter ψ is defined by the ratio of the amplitudes of the Fresnel coefficients:

$$\tan \psi = \frac{\rho_n}{\rho_p} \tag{8a}$$

and the ellipsometric parameter Δ by the difference of their phases:

$$\Delta = \phi_p - \phi_n \tag{8b}$$

The ratio η is defined by

$$\eta = \frac{\hat{r}_p}{\hat{r}_n} = \tan \psi e^{i\Delta} \tag{9}$$

The complex index of refraction of the reflecting surface is derived from the ellipsometric parameters, the angle of incidence Θ_1, and the refractive index n_1 of the first medium by means of the following equation:

$$n_2 - ik_2 = n_1 \tan \Theta_i \sqrt{1 - \frac{4\eta \sin^2 \Theta_i}{(1+\eta^2)}} \tag{10}$$

Equation (10) is only valid if the medium in which the incident and reflected wave propagates (medium 1) is a dielectric. Through separation in real and imaginary parts the refractive index n_2 and the extinction

coefficient k_2 are obtained. The reflectivity $\mathfrak{R}_\perp$ of the sample for normal incidence (given by Eq. (3)) is obtained by

$$\mathfrak{R}_\perp = \frac{|R|^2}{|A|^2} = \frac{(n_1 - n_2)^2 + k_2^2}{(n_1 + n_2)^2 + k_2^2} \tag{11}$$

From the law of the conservation of energy $\mathfrak{R} + \mathfrak{A} + \mathfrak{T} = 1$ (where $\mathfrak{R}$ is the reflectivity, $\mathfrak{A}$ is the absorptivity and $\mathfrak{T}$ is the transmittance) and Kirchhoff's law for normal incidence $\varepsilon_\perp = \mathfrak{A}_\perp$ one arrives at

$$\varepsilon_\perp = 1 - \mathfrak{R}_\perp = \frac{4n_1 n_2}{(n_1^2 + n_2^2) + k_2^2} \tag{12}$$

for the normal spectral emissivity at the laser wavelength. Equation (12) is only valid for opaque materials, where the transmittance $\mathfrak{T}$ is zero.

4. DIVISION-OF-AMPLITUDE PHOTOPOLARIMETER

The division-of-amplitude photopolarimeter (μ-DOAP) [4] consists of the following components: the light source, the polarization state generator (PSG), the polarization state detector (PSD), and the electronics to amplify and record the measurement signals (Fig. 3). The light source is a laser diode emitting at 684.5 nm, which is amplitude-modulated with an 8 MHz square wave. To obtain a circular and Gaussian-shaped beam profile, the

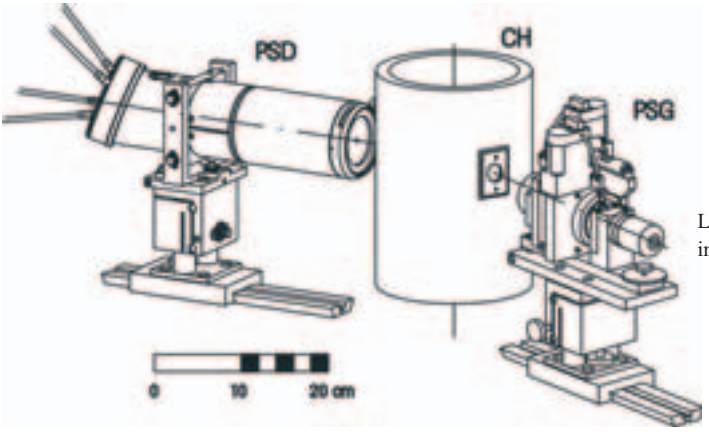

Fig. 3. Division-of-amplitude photopolarimeter. PSG, polarization state generator; PSD, polarization state detector; CH, experimental chamber.

emitted beam is corrected by a pair of anamorphic prisms and a suitable combination of lenses. The output power of the laser after these components is about 25 mW.

The PSG module essentially consists of a linear polarizer and a quarter wave retarder that are mounted in motorized rotation stages. Any polarization state can be generated by suitable angular position of these two components. The two rotation stages are computer-controlled via the DOAP-software.

The PSD module is the main part of the polarimeter. In this detector the reflected light is first collimated by means of a pair of lenses, and then split into two beams by a coated beam splitter. These two beams are split again by two Glan–Thompson prisms with a suitable choice of the coating and the angle of the beam splitter relative to the axis of the beam [5, 6]. The four resulting beams are focused onto four light guides which deliver the light into an electromagnetically shielded room, where it is detected by four silicon photodetectors and amplified by the lock-in technique. An interference filter that is centered at 684.5 nm and located behind the first lens of the PSD is used to suppress most of the background radiation that is emitted by the hot sample surface.

Figure 4 shows the optical components of the μ-DOAP. The PSG module and the light source are shown to the left of the sample, the right part shows the PSD. The CCD camera is used for alignment.

The Stokes vector of the reflected light is computed from the four measured intensities $\vec{I} = (I_0, I_1, I_2, I_3)$ by means of the 4×4 instrument matrix $\overleftrightarrow{A}$:

$$\vec{S} = \overleftrightarrow{A}^{-1} \cdot \vec{I} \tag{13}$$

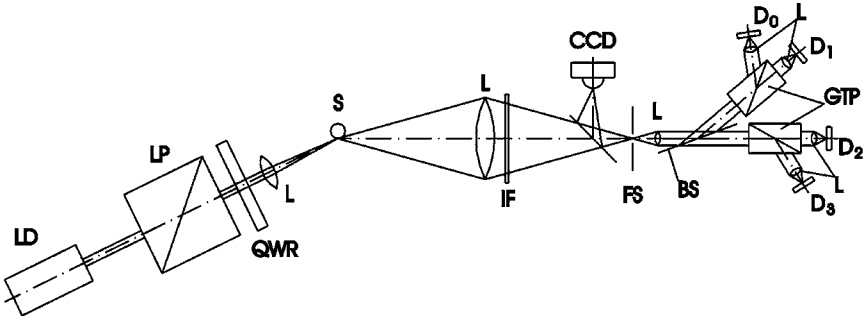

Fig. 4. Optical components of the μ-DOAP. LD, laser diode; LP, linear polarizer; QWR, quarter wave retarder; S, sample; L, lens; IF, interference filter; CCD, CCD camera; FS, field stop; BS, beam splitter; GTP, Glann–Thompson prism; D, detector.

The instrument matrix $\vec{\vec{A}}$ is obtained by a calibration of the DOAP. During calibration the PSG module is mounted opposite to the PSD. Thirty-six linearly polarized and 18 left- and 18 right-handed circularly polarized states are generated with the PSG. From the measured intensities the instrument matrix is determined using statistical methods [7–9]. Since the laser beam is already polarized before the entry into the PSG module, the intensity of the beam after the PSG depends on the generated state of polarization. To correct for this effect, the intensity after the PSG module is measured by a polarization preserving detector module and the measured signals are then normalized with respect to the signal of this detector. To verify the result of the calibration and to realize an angle of 140°, the laser is reflected on a prism made of BK7 glass. After calibration the PSG is moved to the measurement position with an angle of 140° between the incident and reflected beams; the angle of incidence is then 70°. A custom-made prism of BK7 glass is used to perform this alignment. Finally, to verify the quality of the calibration, the index of refraction of the glass prism is measured with the polarimeter, typically within 0.5% of the published value.

For an incident beam that is linearly polarized at 45° relative to the plane of incidence the ellipsometric parameters can be calculated from the measured Stokes vector of the reflected beam as follows:

$$\tan \Delta = \frac{-S_3'}{S_2'} \tag{14}$$

$$\tan 2\psi = \frac{\sqrt{S_2'^2 + S_3'^2}}{-S_1'} \tag{15}$$

The normal spectral emissivity is obtained by combining Eqs. (13)–(15) with Eqs. (10) and (12).

5. RESULTS

To avoid getting some laser straylight into the pyrometer, the used pyrometer operates at a center wavelength of 650 nm with a full-width-at-half-maximum (FWHM) bandwidth of 37 nm. No correction was applied to the data to account for the small difference in operating wavelengths between the pyrometer and the polarimeter.

Figure 5 shows the four measured DOAP intensities for a single experiment on tantalum. At about 20 μs the sample melts and, due to the instant smoothing of the surface, its reflectance, and therefore the polarimeter signals, increase. In the liquid phase ($t = 20$ to 35 μs) the signals show

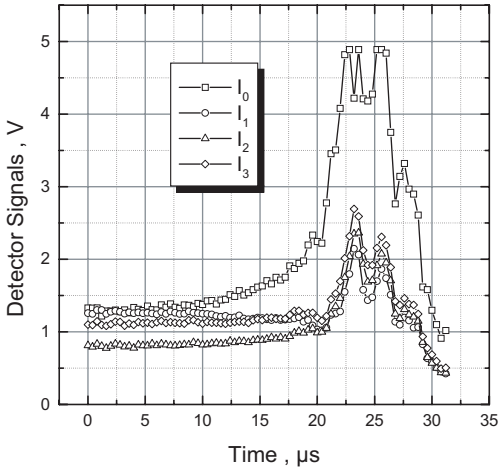

Fig. 5. The four detector signals of the DOAP for a typical experiment on tantalum as a function of time.

a strong and correlated fluctuation. In an earlier publication [10] the non-Gaussian profile of the laser was assumed to be responsible for these signal oscillations. However, although a different laser system with a nice Gaussian beam shape was used for this work, the oscillations were observed again. This eliminates the laser as a source of these oscillations. We now believe that these fluctuations are caused by fast oscillations of the sample surface due to magneto-hydrodynamic instabilities [11]. This might result in a not perfect spatial correlation of the four intensities at the entrances of the four lightguides, as discussed in Ref. 18. Unfortunately, these fluctuations do not cancel out completely in the computed emissivity data.

Figure 6 shows the normal spectral emissivity of tantalum as a function of radiance temperature. The data in the solid phase depend strongly on the pre-treatment of the sample surface (roughness and presence of oxide layers), which is why all the samples were treated with a very fine abrasive paper. Still the reproducibility of the data in the solid phase is very poor. The value at the melting transition for comparison is calculated and interpolated from radiance temperatures [12]. Values in the solid phase strongly depend on surface conditions and therefore are not very reliable. In the liquid phase, the normal spectral emissivity of tantalum decreases substantially with increasing temperature. This means, that the improvement in the accuracy of our temperature measurement due to the polarimeter is significant. Compared to the assumption of a constant emissivity in the liquid phase the difference in true temperature at 5000 K is 8%.

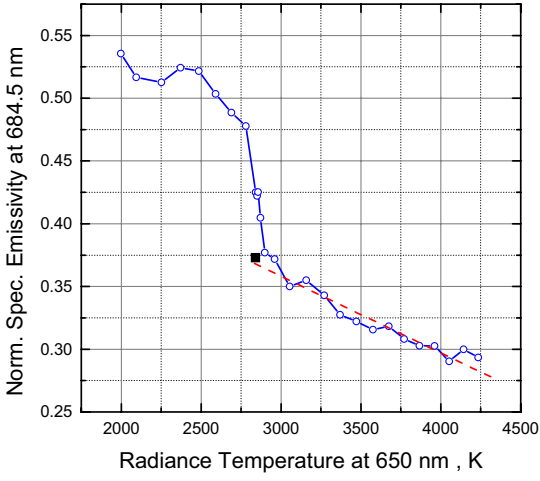

Fig. 6. Normal spectral emissivity (at 684.5 nm) of tantalum as a function of radiance temperature (at 650 nm). Solid line: average of 7 experiments, square: value at the melting point calculated from radiance temperatures from Ref. 12, dashed line: linear fit to experimental results.

Improved data on the thermophysical properties of tantalum and tungsten are presented in Refs. 1 and 13, respectively.

The normal spectral emissivity of niobium as a function of radiance temperature is shown in Fig. 7. The constant value of 0.55 in the solid state represents the average value of eight experiments. The dashed line represents results from Ref. 14, measured with a similar fast polarimeter at NIST. The square represents the normal spectral emissivity at melting, calculated and interpolated from published radiance temperatures at melting [15] at wavelengths close to 684.5 nm. In the solid state the normal spectral emissivity stays constant within our measurement uncertainty.

The results on nickel are shown in Fig. 8. The lower limiting radiance temperature of the pyrometer is about 1400 K, so data are only presented for the liquid state. The square again represents the value at the melting point calculated and interpolated from radiance temperatures at melting from Ref. 16. For liquid nickel the emissivity increases with increasing temperature.

Figure 9 shows the normal spectral emissivity of tungsten at 684.5 nm as a function of radiance temperature. For this material the emissivity in the liquid decreases with increasing temperature, but the decrease is not as large as in the case of tantalum.

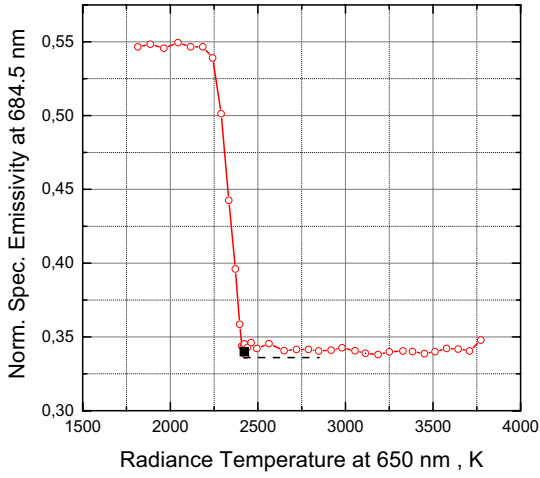

Fig. 7. Normal spectral emissivity (at 684.5 nm) of niobium as a function of radiance temperature (at 650 nm). Dashed line: results from Ref. 14, square: value at the melting point calculated from radiance temperature from Ref. 15.

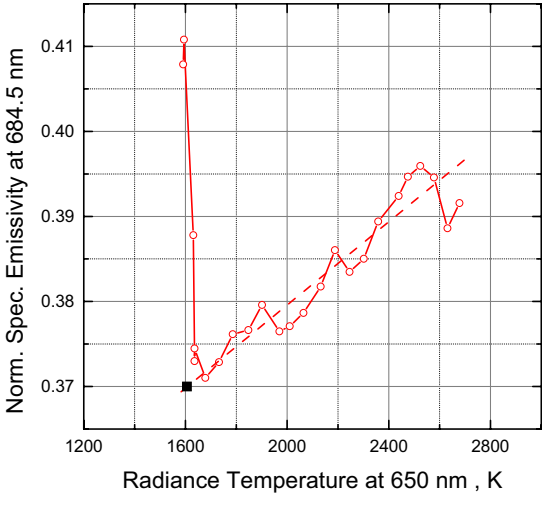

Fig. 8. Normal spectral emissivity (at 684.5 nm) of nickel as a function of radiance temperature (at 650 nm). Square: value at the melting point calculated from radiance temperature from Ref. 16, dashed line: linear fit to experimental results.

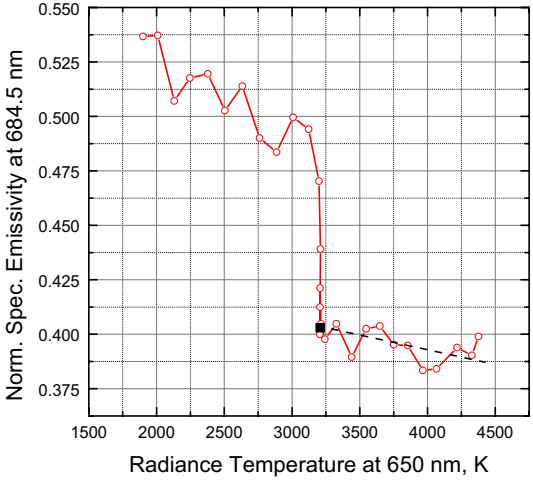

Fig. 9. Normal spectral emissivity (at 684.5 nm) of tungsten as a function of radiance temperature (at 650 nm). Square: value at the melting point calculated from radiance temperature from Ref. 17, dashed line: linear fit to experimental results.

The least-squares fits for the normal spectral emissivity as a function of radiance temperature for all materials presented in this paper are given in Table I.

6. MEASUREMENT UNCERTAINTIES

In this work a coverage factor of $k = 2$ was used, and thus the reported expanded uncertainties represent two-standard-deviation estimates [19]. The uncertainty in radiance temperature is 2% at the end of the stable liquid phase, whereas the uncertainty in normal spectral emissivity in the liquid state is 6%. The uncertainty in true temperature does not exceed 4%

Table I. Least-Squares fits for the Normal Spectral Emissivity at 684.5 nm of the Investigated Materials as a Function of Radiance Temperature at 650 nm in the Form $\varepsilon_\perp = a + bT$ (K)

Material	Temp. Range (K)	a	b (K^{-1})
Tantalum	$2850 < T < 4300$	0.545	-6.16×10^{-5}
Niobium	$2450 < T < 3700$	0.345	0
Nickel	$1610 < T < 2700$	0.33	2.45×10^{-5}
Tungsten	$2850 < T < 4400$	0.44	-1.19×10^{-5}

at the end of the liquid phase. This includes the error caused by the difference in operating wavelengths between the pyrometer and the polarimeter.

7. CONCLUSION

This work presents results of the normal spectral emissivity at 684.5 nm of several liquid metals at temperatures up to 5000 K. These measurements have been made possible by the use of a fast polarimeter in conjunction with a pulse-heating system. These results indicate that the emissivity of liquid metals can increase, decrease or even remain constant with increasing temperature. The work demonstrates that it is important to measure the normal spectral emissivity of a sample simultaneously with its radiance temperature in order to avoid large uncertainties in the computed true temperature.

ACKNOWLEDGMENT

This work was supported by the "Austrian Fonds zur Förderung der wissenschaftlichen Forschung (FWF)" Grant P12775-PHY.

REFERENCES

1. A. Seifter, S. Krishnan, and G. Pottlacher, *Proceedings of Tempmeko 2001* (VDE Verlag GMBH, Berlin, 2001), p. 307.
2. R. M. A. Azzam, *Ellipsometry and Polarized Light* (North-Holland, New York, 1987).
3. M. Born and E. Wolf, *Principles of Optics,* 7th Ed. (Cambridge University Press, 1999).
4. R. M. A. Azzam, *Opt. Acta* **29**:685 (1982).
5. K. Brudzewski, *J. Mod. Opts.* **38**:889 (1991).
6. R. M. A. Azzam, *Opt. Acta* **32**:1407 (1985).
7. R. M. A. Azzam, E. Masetti, M. Elminyawi, and A. M. El-Saba, *Rev. Sci. Instrum.* **59**:84 (1988).
8. R. M. A. Azzam and A. G. Lopez, *J. Opt. Soc. Am.* **A6**:1513 (1989).
9. S. Krishnan, *J. Opt. Soc. Am.* **A9**:1615 (1992).
10. A. Seifter, F. Sachsenhofer, S. Krishnan, and G. Pottlacher, *Int. J. Thermophys.* **22**:1537 (2001).
11. U. Seydel, W. Fucke, and H. Wadle, *Die Bestimmung thermophysikalischer Daten flüssiger hochschmelzender Metalle mit schnellen Pulsaufheizexperimenten* (Verlag Dr. Peter Mannhold, Düsseldorf, 1980).
12. A. Cezairliyan, J. McClure, L. Coslovi, F. Righini, and A. Rosso, *High Temp.-High Press.* **8**:103 (1976).
13. A. Seifter and G. Pottlacher, *Int. J. Thermophys.* **23**:1281 (2002).
14. K. Boboridis, *Application of Single-Wavelength Radiation Thermometry and High-Speed Laser Polarimetry to Thermophysical Property Measurements on Pulse-Heated Materials*, Dissertation, TU–Graz (2001).
15. A. Cezairliyan and A. P. Miiller, *Int. J. Thermophys.* **13**:39 (1992).

16. E. Kaschnitz, J. L. McClure, and A. Cezairliyan, *Int. J. Thermophys.* **19**:1637 (1998).
17. A. Cezairliyan and A. P. Miiller, *Int. J. Thermophys.* **3**:89 (1982).
18. A. Seifter, *Bestimmung des normalen spektralen Emissionskoeffizienten von flüssigen pulsgeheizten metallen Mittels eines schnellen Photopolarimeters*, Dissertation, TU–Graz (2001).
19. DIN, Deutsches Institut für Normung, e.V., *Guide to the Expression of Uncertainty in Measurement* (Verlag Beuth, Berlin 1995).